Organic Electronics 12 (2011) 2192–2197

Contents lists available at SciVerse ScienceDirect

Organic Electronics

journal homepage: www.elsevier.com/locate/orgel

Semitransparent white organic light-emitting devices with symmetrical electrode structure

Wenyu Ji [a,b,c], Letian Zhang [b], Kai Xu [b], Wenfa Xie [b,*], Hanzhuang Zhang [c], Guoqiang Liu [c], Jinbo Yao [d]

[a] Key Laboratory of Excited State Processes, Changchun Institute of Optics, Fine Mechanics and Physics, Chinese Academy of Sciences, Changchun 130033, People's Republic of China
[b] State Key Laboratory on Integrated Optoelectronics, College of Electronic Science and Engineering, Jilin University, Changchun 130012, People's Republic of China
[c] Department of Physics, Jilin University, Changchun 130023, People's Republic of China
[d] The Fundamental Training Base of Aviation University of Air Force, Changchun 130023, People's Republic of China

ARTICLE INFO

Article history:
Received 6 July 2011
Received in revised form 17 September 2011
Accepted 17 September 2011
Available online 1 October 2011

Keywords:
Semitransparent
White organic light-emitting device
Symmetrical electrode

ABSTRACT

A semitransparent white-light organic light-emitting device (SWOLED) with an $(Ag/Alq_3)_2$ cathode and $(Alq_3/Ag)_2$ anode was fabricated. The light emitted from the emitters subjecting to the same propagation process because of the symmetrical electrode structure. The device showed few differences in luminance, power distribution of electroluminescence (EL) spectra, efficiency and chromaticity coordinates from both sides. The maximum total current efficiency of the SWOLED (8.46 cd/A) is comparable to that of the corresponding bottom-emitting OLED (9.2 cd/A). The SWOLEDs have potential uses as tinted thin-film coatings on architectural surfaces, such as windows and walls. In addition, this kind of electrode can be used in flexible OLEDs.

White organic light-emitting devices (OLEDs), have aroused much attention in the past decade because of their potential uses in full color flat-panel displays (FPDs), automobile, and lighting source [1,2]. One of the advantages of OLEDs, compared with other display technologies, is the possibility of making flexible displays [3–6]. In particular, transparent/semitransparent organic light-emitting devices (T/SOLEDs) or top-emitting OLEDs have much more advantages than the bottom-emitting ones in FPDs and solid-state lighting due to high aperture ratio and low cost. T/SOLEDs or top-emitting OLEDs based on tris(8-hydroxyquinoline) aluminum (Alq_3) have also been reported [7–11]. However, there are only a few reports on the white top-emitting OLEDs or white T/SOLEDs [12–17]. Considerable efforts have been devoted to design the structure of anode and cathode in T/SOLEDs [8,9,11,13,18–23]. Gu et al. reported T/SOLEDs with indium tin oxide (ITO) as an anode and Mg:Ag as a semitransparent cathode [8]. It is worth noting that the ratio of Mg and Ag, which affects the transmittance of the cathode, is a key factor to the performance of devices. Unfortunately, the reproducibility of device is poor because it is difficult to precisely control the ratio of Mg and Ag in the vapor deposition process of cathode. In the case of T/SOLEDs with ITO and Mg:Ag as electrodes, the total efficiency of the device is almost constant irrespective of the composition of the cathode [24]. The reflectance of the cathode only affects the relative ratio of the light intensity through anode and cathode without adjusting the chromaticity coordinates and total light emission in the devices. Xie et al. reported a transparent OLED with ITO anode and Yb:Ag cathode [25], which showed few differences in luminance from both sides of the device. But there exists the same problem as Mg:Ag cathode case. In addition, the transparent inverted OLED with ITO as both anode and cathode was reported [26]. The WO_3 layer has to be applied as a buffer layer to prevent the hole-transport layer from damaging in sputtering

* Corresponding author.
E-mail address: xiewf@jlu.edu.cn (W. Xie).

1566-1199/$ - see front matter © 2011 Elsevier B.V. All rights reserved.
doi:10.1016/j.orgel.2011.09.011

process of ITO thin film and sputtering process also increases the complexity of device fabrication.

Although many efforts have been made on the T/SOLEDs, fabricating white T/SOLEDs with microcavity effects still leaves a door open. The difference in luminance, efficiency and chromaticity coordinates for the emission from both sides was hardly avoided in T/SOLEDs owing to an asymmetric structure of light propagation. In this article, we designed and fabricated a new type of SWOLED with the same electrode composition of a semitransparent multilayer of $(Ag/Alq_3)_2$ and $(Alq_3/Ag)_2$ as the cathode and anode, respectively. The device showed few differences in luminance, efficiency and spectra from both sides. Furthermore, this kind of electrode can be potentially fabricated on the soft substrate for flexible OLEDs, like the similar structure electrodes (for example, ITO/Ag/ITO, Al/Alq_3/Al, ZnS/Ag/WO_3) utilized in flexible OLEDs [27–29].

We designed SWOLED (device A) consisting of glass substrate/$(Alq_3/Ag)_n$/MoO_3 (1.5 nm)/4,4′,4″-tris(3-methylphenyl-phenylamino)-triphenylamine (*m*-MTDATA, 30 nm)/*N*,*N*′-bis-(1-naphthyl)-*N*,*N*′-diphenyl-1, 1-biphenyl-4,4′-diamine (NPB, 10 nm)/4,4′-bis(2,2′-diphenylvinyl)-1,1′-biphenyl (DPVBi, 15 nm)/4,4-*N*,*N*-dicarbazole-biphenyl (CBP, 3 nm)/CBP:bis(2-(2-fluorphenyl)-1,3-benzothiozolato-*N*, C2′)iridium(acetylacetonate) [$(F–BT)_2Ir(acac)$] (7 nm)/4,7-diphenyl-1,10-phenanthroline (Bphen, 35 nm)/LiF (1 nm)/Al (1 nm)/$(Ag/Alq_3)_n$. In this device, *m*-MTDATA, NPB, DPVBi, CBP:(F–BT)2Ir(acac), Bphen, and LiF/Al/Ag/M/A/M were used as the hole injection layer (HIL), hole transporting layer (HTL), blue emitting layer, orange emitting layer, electron transporting layer (ETL), respectively. The neat CBP was introduced to separated blue and orange emitting layers to avoid the Dexter energy transfer between the two emitters. For comparison, the bottom-emitting device (ITO glass substrate) with the same organic layers (device B) and 100 nm Al as a cathode was fabricated. The thickness of each layer was optimized according to the analysis below. The deposition of layers and the measure of devices characteristics were described before [16]. The transmission spectrum was measured by means of ultraviolet/visible spectrometer (UV 1700, Shimadzu).

Fig. 1a shows the transmittance and reflectance spectra of the electrodes with different thickness of Alq_3. Considering the transmittance and electrical characteristics of the electrodes, a thin Ag layer can have high transmittance and a thick Ag layer can have high conduction, 22 nm Ag layer is chosen. As can be seen, the peak of transmittance/reflectance shift to longer wavelength as the thickness of Alq_3 increased. As depicted in Ref. [30], two resonant cavity modes are necessary in our devices. In order to obtain high effective microcavity devices, a moderate transmittance and reflectance is need near the resonant wavelengths (RWs) 448 and 590 nm, so 80 or 85 nm Alq_3 is chose. Fig. 1b shows the absorption spectra of the electrodes. We can see that a larger absorption is obtained at long wavelength region. Considering the absorption of the electrodes, 85 nm Alq_3 layer is better due to lower absorption of electrode than that of 80 nm Alq_3.

In addition, we calculated the cavity emission by considering wavelength-independent intrinsic luminescence spectra of the emitters [31] in order to clarify the microcavity effect in the device and optimize the parameters of device A. The peak wavelength of the resonant cavity mode is dependent on the optical thickness of the cavity region and the Bragg peak wavelength of the electrodes [32]. Thus, in order to adjust the position of the resonant peak, we only change the thickness of the hole injection layer and electron transporting layer and hold other layers constant when altering the optical thickness of the cavity region. Fig. 2a and b shows the cavity emission from Ag side (cathode side) and glass side (anode side), respectively. Different thickness active layers, 90, 100, 110, 130, and 150 nm are adopted and the thickness of the electrodes is constant, 22 and 85 nm for Ag and Alq_3, respectively. We can see that two resonant peaks are obtained and the RWs shift towards longer wavelength region with the active layers thickness increasing. In order to obtain high effective device we choose the thickness of 100 nm for active layers considering the emission peaks of blue (DPVBi, emission peak at 448 nm) and yellow [$(F–BT)_2Ir(acac)$, emission peak at 548 and a shoulder peak at 590 nm] emitters. Meanwhile, we can see that almost the same emission can be obtained from both sides of the device.

In addition, we can also confirm the position of the resonant peak by utilizing the Fabry–Perot peak condition

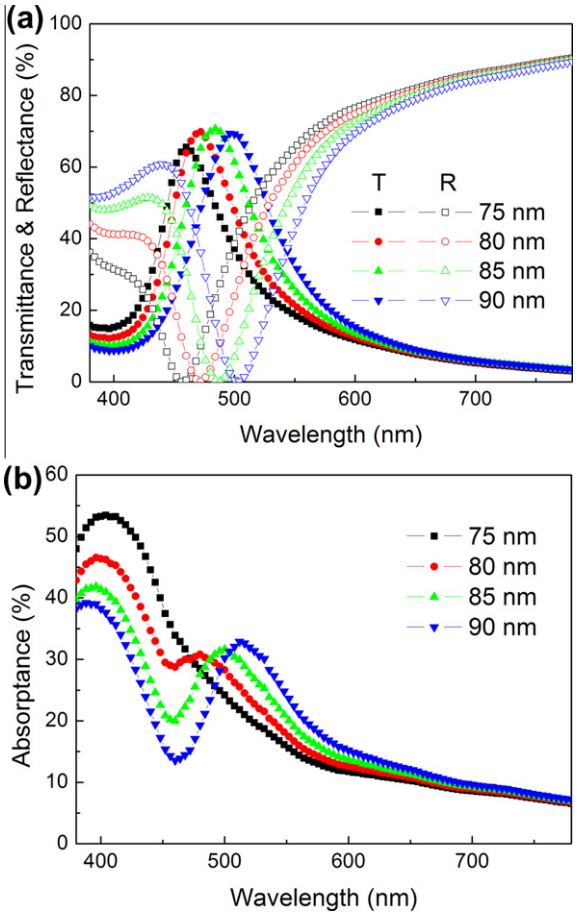

Fig. 1. (a) The transmittance, reflectance and (b) absorption spectra of the electrodes with different Alq_3 thickness.

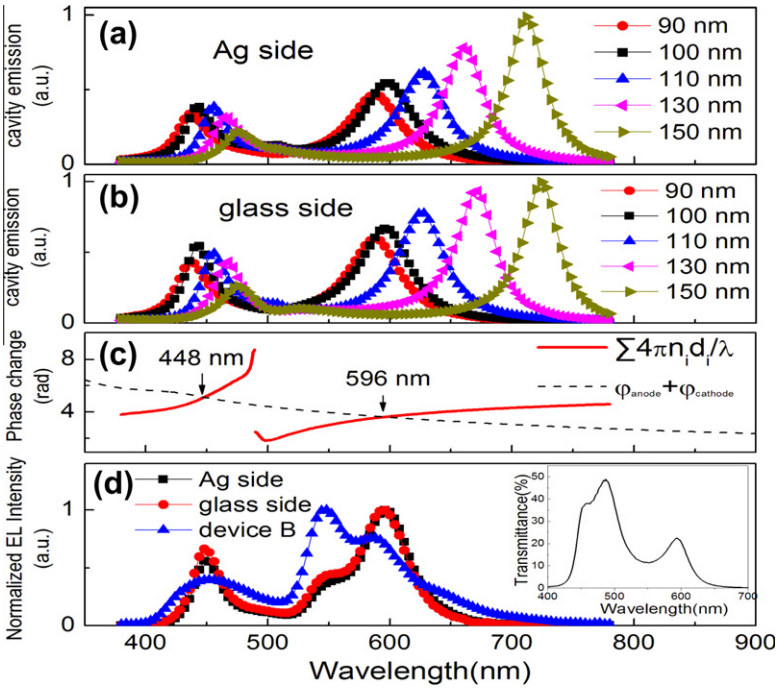

Fig. 2. The cavity emission from (a) Ag side (cathode) and (b) glass side (anode) with different thickness active layers; (c) the calculated round-trip phase changes for 100 nm organic layers between two electrodes and the phase changes for two electrodes; (d) the normalized measured EL spectra for devices A and B. Inset is the measured transmission for device A.

[33]. The resonant wavelength (RW) condition of the microcavity for normal incidence is determined by the below equation:

$$\sum_i \frac{4\pi d_i n_i(\lambda)}{\lambda} - \varphi_{\text{cathode}}(0,\lambda) - \varphi_{\text{anode}}(0,\lambda) = 2m\pi$$

where λ is the emission wavelength, $\varphi_{\text{cathode}}(0, \lambda)$ and $\varphi_{\text{anode}}(0, \lambda)$ are the angle- and the wavelength-dependent phase changes on reflection from top cathode and bottom anode, respectively, and m is an integer that defines the mode number (in our work, we choose $m = 0$), $n_i(\lambda)$ and d_i are the refractive index and thickness of organic layers.

Fig. 2c shows the calculated round-trip phase changes for 100 nm organic layers sandwiched between two reflection electrodes [i.e., $\varphi_1(\lambda) = \Sigma 4\pi n_i(\lambda) d_i/\lambda$], and the phase shift at two reflective electrodes [i.e., $\varphi_2(\lambda) = \varphi_{\text{cathode}}(\lambda) + \varphi_{\text{anode}}(\lambda)$] in forward direction. The points of the intersection of $\varphi_1(\lambda)$ and $\varphi_2(\lambda)$ are the RWs of the device. Two RWs at 448 and 596 nm will occur in the designed device. The detail calculations were described before [14,15]. Fig. 2d shows the normalized measured EL spectra at voltage of 8 V for devices A and B in forward direction. The spectrum of the device B shows two main peaks at 448 and 548 nm originating from DPVBi and $(F–BT)_2Ir(acac)$, respectively. The shoulder peak is at 590 nm. Device A shows two resonant emission peaks at 448 and 596 nm for both sides, which are in excellent agreement with the calculated results. It can be seen that the spectra for Ag- and glass-side have only little difference. In other words, we can obtain almost the same emission from both sides with this structure. Comparing these two devices, the narrower full width at half maximum (FWHM) of the DPVBi and $(F–BT)_2Ir(acac)$ emission in device A is observed (for example, the FWHM of the $(F–BT)_2Ir(acac)$ is 90 nm for device B and 28 nm for device A). This result also indicates that strong microcavity effect is occurred in this SWOLED. Inset shows the measured transmittance of the device in forward direction. As can be seen, the device has two transmission peaks at 487 and 592 nm and a shoulder peak at 456 nm, which is the characteristic of periodic structure electrodes.

Fig. 3a and b shows the normalized EL spectra at viewing angle of 0°, 30°, and 60° and a voltage of 8 V for Ag side and glass side, respectively. As can be seen, the experiment results (solid symbols) are in excellent agreement with the simulated results (open symbols) and the details of calculation is described before [16]. With the viewing angle increasing, the RWs shift to a shorter wavelength due to the microcavity effect for either Ag side (upper) or glass side (down). A white emission was obtained with CIE coordinates (0.424 and 0.347) [(0.402 and 0.344)] at a viewing angle of 0° and changing to (0.419 and 0.379) [(0.399 and 0.376)] at 30° and (0.368 and 0.456) [(0.351 and 0.458)] at 60° for Ag side (glass side). Fig. 4a and b shows the normalized measured EL spectra at voltage of 6, 8, and 10 V for device A in forward direction, for Ag side and glass side, respectively. We can see that the spectra are fairly stable over a range of operation voltages for both sides. In other words, the CIE coordinates are stable within the operation voltage, which are very important in displays and lighting. Fig. 3c indicates the measured angular distribution of the

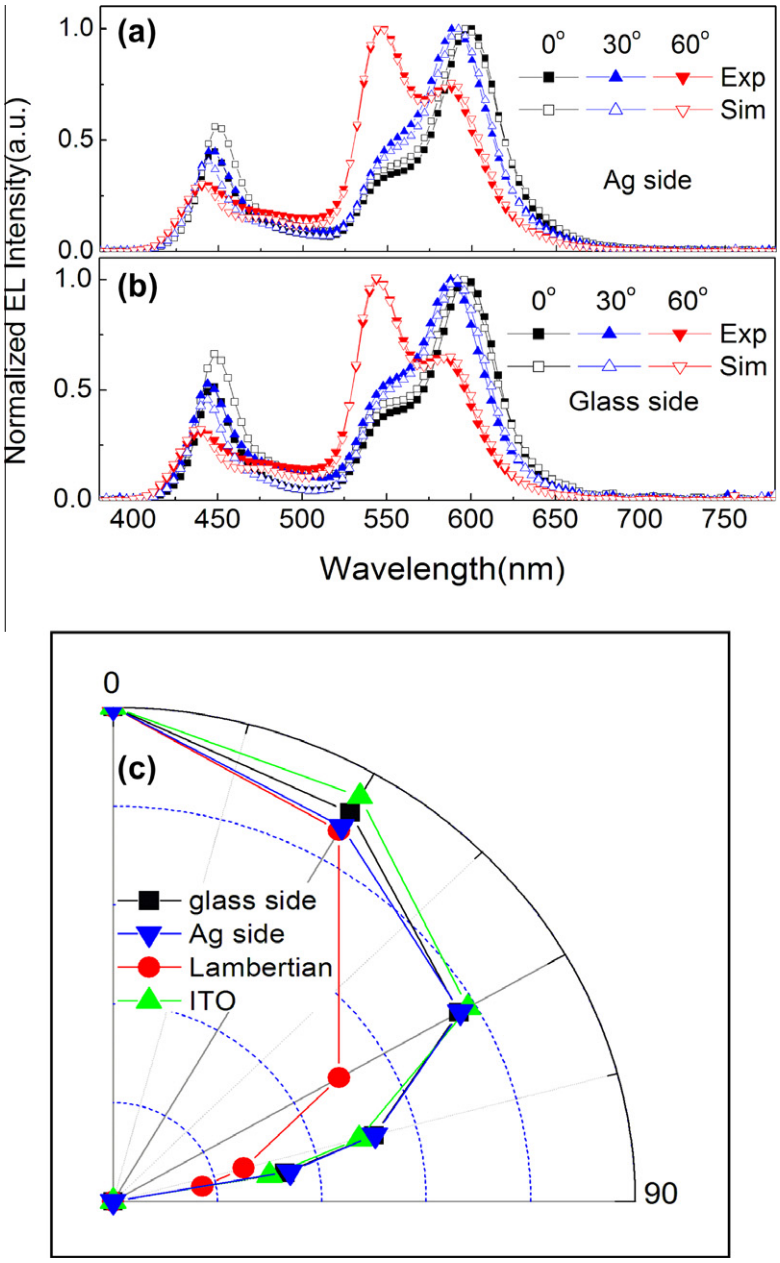

Fig. 3. (a) The normalized experimental (Exp) and simulated (Sim) EL spectra at different viewing angles and voltage of 8 V for (a) Ag side and (b) glass side; (c) the measured angular distribution of the devices and the red solid circle represents a Lambertian-type distribution. (For interpretation of the references to color in this figure legend, the reader is referred to the web version of this article.)

devices and the red solid circle represents a Lambertian-type distribution. We can see that the emission of SWOLED has the similar angular distribution as that of ITO-based OLED, which is a super-Lambertian distribution [16].

Fig. 5a shows the current density–luminance–voltage characteristics of the SWOLED. There is only little difference in luminance from both sides. For example, at the driving voltage of 10 V, the luminance for the Ag side and glass side is 2550 and 2423 cd/m^2, respectively. Fig. 4b shows the forward direction efficiency of the device A and B. The maximum efficiencies from Ag side and glass side of the SWOLED are 4.14 and 4.32 cd/A, respectively. The maximum total EL efficiency of the device is 8.46 cd/A, which is comparable to the corresponding bottom-emitting WOLED (9.20 cd/A).

Fig. 6 shows the transmittance, reflectance, and absorption spectra of the cathode (electrode 1) and anode (electrode 2). As can be seen, the two electrodes almost have the same spectral response, which ensures the uniform optical characteristics of the two sides for the SWOLED.

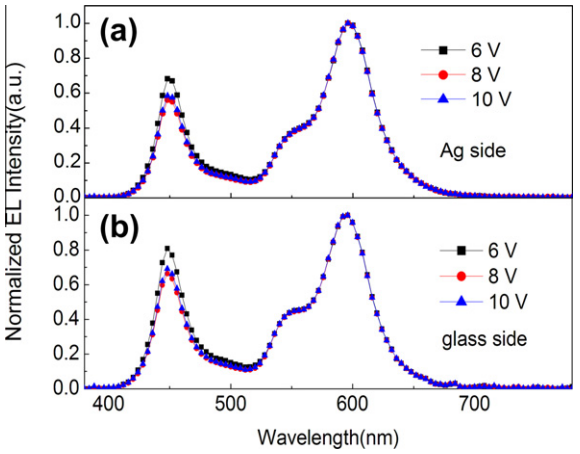

Fig. 4. The normalized measured EL spectra of device A at voltage of 6, 8, and 10 V, (a) Ag side and (b) glass side.

The loss due to the absorption by multilayer electrode is about 30%. The absorption at the RW is 20% (RW = 448 nm) and 15% (RW = 596 nm). Fig. 7 shows the ratio of air mode, glass mode, and nonemissive mode (waveguide mode and surface plasmon polaritons) to the total emission as a function of wavelength simulated by numerical method of the finite-difference time-domain (FDTD) [34]. The inset is the normalized PL spectra of the DPVBi and

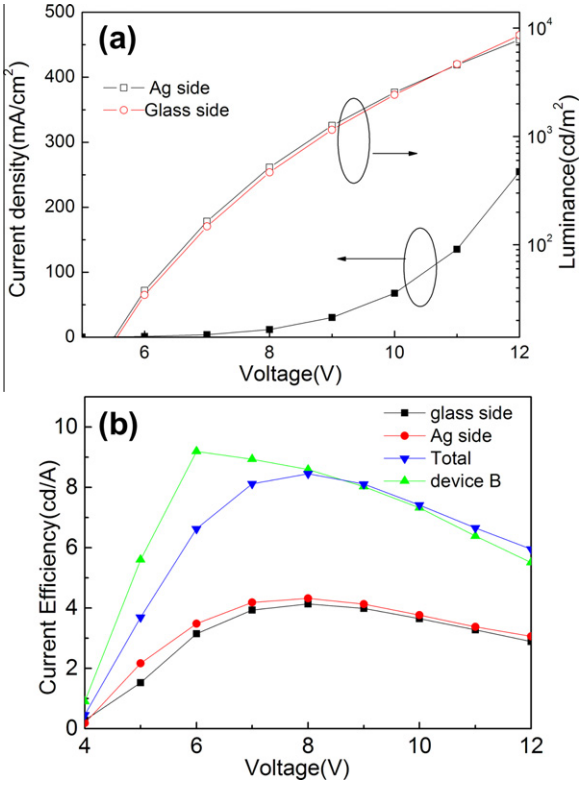

Fig. 5. (a) The voltage–current density–luminance characteristics of the devices; (b) the efficiency–voltage characteristics.

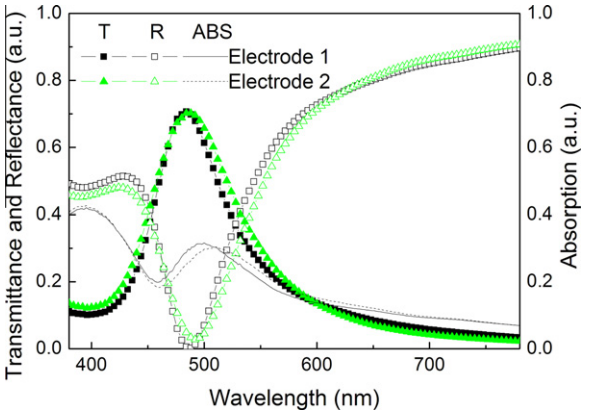

Fig. 6. The transmittance, reflectance and absorption spectra of the electrodes.

CBP:$(F–BT)_2Ir(acac)$. Thus, the light extraction efficiency of the SWOLED could be defined as $\eta_{ext} = \int_{380}^{780}[k_1 S_b(\lambda) + (1-k_1)S_y(\lambda)]\eta_{air}(\lambda)d\lambda$, where k_1 is the weight of the blue emission to the white emission. $S_b(\lambda)$ and $S_y(\lambda)$ are the photoluminescence (PL) spectrum normalized with its area of the blue and yellow emitting material. $\eta_{air}(\lambda)$ is the air mode of the SWOLED as function of wavelength. According to the EL spectra of the SWOLED, the weight of the blue emission to the white emission is about 40%. Thus, the calculated light extraction efficiency of the SWOLED is 11.3% which is less than that of the bottom device (~20%). However, the radiative quantum efficiency of the emissive materials will increase in the microcavity device due to the presence of the Purcell effect [35]. The calculated Purcell factor for the blue and yellow emitting material is 2.3 and 3.2 in the SWOLED, respectively. The PL quantum efficiency of DPVBi and CBP: $(F–BT)_2Ir(acac)$ are 0.4 and 0.62. Then, the improvement of the radiative quantum efficiency of DPVBi and $(F–BT)_2Ir(acac)$ is about 50% and 35%, respectively. As a result, the efficiency of the SWOLED is comparable to that of the corresponding bottom-emitting OLED.

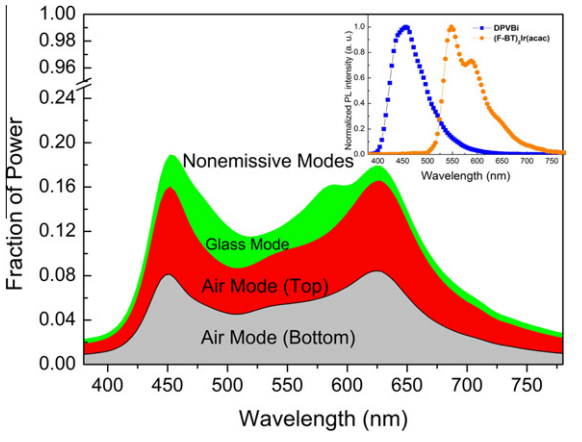

Fig. 7. The ratio of air mode, glass mode, and nonemissive mode to the total emission as a function of wavelength.

In summary, the SWOLED with $(Ag/Alq_3)_2$ electrodes was demonstrated, which showed few differences in luminance, spectra and efficiency. The total efficiency of the SWOLED is comparable to the corresponding bottom-emitting OLED. By changing optical thickness of the cavity region, we can adjust the RWs of the device. In fact, we can also adjust the optical characteristics (including the RWs and transmittance) of the device by adjusting the parameters of the electrodes. The results will provide guidance in fabrication of OLEDs with optimum performance, such as high efficiency, pure color emission, required transmittance, and flexible devices. At present, the SWOLEDs have the cavity effect which leads to an angular dependent EL emission. However, the devices can be used as the screens of mobile phones and smartphones that do not need high quality at a large viewing angle.

Acknowledgments

This work was supported by the National Natural Science Foundation of China (Grant Nos. 60937001, 11074096, 61077045, 61177026, 60723002, 10774060, and 10974071) and New Century Excellent Talents in University (No. 100446).

References

[1] R.H. Jordan, A. Dodabalapur, M. Strukeji, Appl. Phys. Lett. 68 (1996) 1192.
[2] H. Mattoussi, H. Murata, C.D. Merritt, Y. Lizumi, J. Kido, Z.H. Kafafi, J. Appl. Phys. 86 (1999) 2642.
[3] G. Gustafsson, Y. Cao, G.M. Treacy, F. Klavetter, N. Colaneri, A.J. Heeger, Nature 357 (1992) 477.
[4] G. Gu, P.E. Burrows, S. Venkatesh, S.R. Forrest, M.E. Thompson, Opt. Lett. 22 (1997) 172.
[5] A.B. Chwang, M.A. Rothman, S.Y. Mao, R.H. Hewitt, M.S. Weaver, J.A. Silvernail, K. Rajan, M. Hack, J.J. Brown, X. Chu, L. Moro, T. Krajewski, N. Rutherford, Appl. Phys. Lett. 83 (2003) 413.
[6] J.S. Lewis, M.S. Weaver, IEEE J. Sel. Top. Quant. 10 (2004) 45.
[7] B.J. Chen, X.W. Sun, S.C. Tan, Opt. Express 13 (2005) 937.
[8] G. Gu, V. Bulović, P.E. Burrows, S.R. Forrest, M.E. Thompson, Appl. Phys. Lett. 68 (1996) 2606.
[9] A. Yamamori, S. Hayashi, T. Koyama, Y. Taniguchi, Appl. Phys. Lett. 78 (2001) 3343.
[10] G. Parthasarathy, C. Adachi, P.E. Burrows, S.R. Forrest, Appl. Phys. Lett. 76 (2000) 2128.
[11] G. Parthasarathy, P.E. Burrows, V. Khalfin, V.G. Kozlov, S.R. Forrest, Appl. Phys. Lett. 72 (1998) 2138.
[12] S.F. Hsu, C.C. Lee, S.W. Hwang, C.H. Chen, Appl. Phys. Lett. 86 (2005) 253508.
[13] H. Kanno, Y. Sun, S.R. Forrest, Appl. Phys. Lett. 86 (2005) 263502.
[14] W.Y. Ji, L.T. Zhang, T.Y. Zhang, G.Q. Liu, W.F. Xie, S.Y. Liu, H.Z. Zhang, L.Y. Zhang, B. Li, Opt. Lett. 34 (2009) 2703.
[15] W.Y. Ji, L.T. Zhang, T.Y. Zhang, W.F. Xie, H.Z. Zhang, Org. Electron. 11 (2009) 202.
[16] W.Y. Ji, L.T. Zhang, R.X. Gao, L.M. Zhang, W.F. Xie, H.Z. Zhang, B. Li, Opt. Express. 16 (2008) 15489.
[17] C.J. Lee, R.B. Pode, J.I. Han, D.G. Moon, Appl. Surf. Sci. 253 (2007) 4249.
[18] P.E. Burrows, V. Khalfin, G. Gu, S.R. Forrest, Appl. Phys. Lett. 73 (1998) 435.
[19] G. Gu, V. Khalfin, S.R. Forrest, Appl. Phys. Lett. 73 (1998) 2399.
[20] G. Gu, G. Parthasarathy, P.E. Burrows, P. Tian, I.G. Hill, A. Kahn, S.R. Forrest, J. Appl. Phys. 86 (1999) 4067.
[21] P.E. Burrows, G. Gu, S.R. Forrest, E.P. Vicenzi, T.X. Zhou, J. Appl. Phys. 87 (2000) 3080.
[22] H. Peng, X. Zhu, J. Sun, Z. Xie, S. Xie, M. Wong, H. Kwok, Appl. Phys. Lett. 87 (2005) 173505.
[23] Q. Huang, K. Walzer, M. Pfeiffer, V. Lyssenko, G. He, K. Leo, Appl. Phys. Lett. 88 (2006) 113515.
[24] J. Meyer, T. Winkler, S. Hamwi, S. Schmale, H.H. Johannes, T. Weimann, P. Hinze, W. Kowlasky, T. Riedl, Adv. Mater. 20 (2008) 3839.
[25] T.Y. Zhang, L.T. Zhang, W.Y. Ji, W.F. Xie, Opt. Lett. 34 (2009) 1174.
[26] M.H. Lu, M.S. Weaver, T.X. Zhou, M. Rothman, R.C. Kwong, M. Hack, J.J. Brown, Appl. Phys. Lett. 81 (2002) 3921.
[27] J. Lewis, S. Grego, B. Chalamala, E. Vick, D. Temple, Appl. Phys. Lett. 85 (2004) 3450.
[28] L. Duan, S. Liu, D. Zhang, J. Qiao, G. Dong, L. Wang, Y. Qiu, J. Phys. D: Appl. Phys. 42 (2009) 075103.
[29] H. Cho, C. Yun, J.W. Park, S. Yoo, Org. Electron. 10 (2009) 1163.
[30] In our work, we achieve white light emission by complementary color, blue (emission peak at 448 nm) and yellow (emission peak at 548 nm). So a cavity with two resonant cavity modes is enough. The device with electrode $(Ag/Alq_3)_2$ can has two peak wavelengths according to our report [Ji et al., Curr. Appl. Phys. 11 (2011) 1410], so we choose $n = 2$ in this work. The peak wavelength of the resonant cavity mode is dependent on the optical thickness of the cavity region and the Bragg peak wavelength of the electrodes as depicted in Ref. [32]. We choose 85 nm Alq_3 layer to make the electrode have two Bragg peak wavelengths near 448 and 590 nm.
[31] P. Freitag, S. Reineke, S. Olthof, M. Furno, B. Lüssem, K. Leo, Org. Electron. 11 (2010) 1676.
[32] D.P. Puzzo, M.G. Helander, P.G. O'Brien, Z.B. Wang, N. Solheilnia, N. Kherani, Z.H. Lu, G.A. Ozin, Nano Lett. 11 (2011) 1457.
[33] A.B. Djurišić, A.D. Rakić, Appl. Opt. 41 (2002) 7650.
[34] A. Chutinan, K. Ishihara, T. Asano, M. Fujita, S. Noda, Org. Electron. 6 (2005) 3.
[35] S. Nowy, B.C. Krummacher, J. Frischeisen, N.A. Reinke, W. Brütting, J. Appl. Phys. 104 (2008) 123109.